ACS APPLIED MATERIALS & INTERFACES

Research Article

www.acsami.org

Tailoring Dielectric Properties and Energy Density of Ferroelectric Polymer Nanocomposites by High-*k* Nanowires

Guanyao Wang,[†] Xingyi Huang,*[,†] and Pingkai Jiang[†,‡]

[†]Department of Polymer Science and Engineering, Shanghai Key Laboratory of Electrical Insulation and Thermal Aging, Shanghai Jiao Tong University, Shanghai 200240, China

[‡]Shanghai Engineering Center for Material Safety of Nuclear Power Equipment, Shanghai 200240, China

Supporting Information

ABSTRACT: High dielectric constant (k) polymer nanocomposites have shown great potential in dielectric and energy storage applications in the past few decades. The introduction of high-k nanomaterials into ferroelectric polymers has proven to be a promising strategy for the fabrication of high-k nanocomposites. One-dimensional large-aspect-ratio nanowires exhibit superiority in enhancing k values and energy density of polymer nanocomposites in comparison to their spherical counterparts. However, the impact of their intrinsic properties on the dielectric properties of polymer nanocomposites has been seldom investigated. Herein, four kinds of nanowires ($Na_2Ti_3O_7$, TiO_2, $BaTiO_3$, and $SrTiO_3$) with different inherent characteristics are elaborately selected to fabricate high-k ferroelectric polymer nanocomposites. Dopamine functionalization facilitates the excellent dispersion of these nanowires in the ferroelectric polymer matrix because of the strong polymer/nanowire interfacial adhesion. A thorough comparative study on the dielectric properties and energy storage capability of the nanowires-based nanocomposites has been presented. The results reveal that, among the four types of nanowires, $BaTiO_3$ NWs show the best potential in improving the energy storage capability of the proposed nanocomposites, resulting from the most signficant increase of k while retaining the rather low dielectric loss and leakage current.

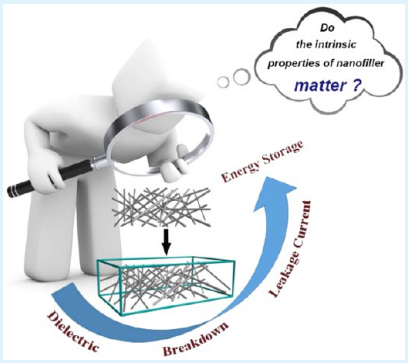

KEYWORDS: *nanowire, nanocomposite, dielectric constant, breakdown strength, energy storage, leakage current*

INTRODUCTION

High dielectric constant (k) materials have drawn tremendous interest for their potential applications in modern electronics and electric power systems such as capacitors, actuators, energy storage devices, and power cable terminations.[1−11] The traditional high-k inorganic ceramic materials, such as TiO_2, $BaTiO_3$, $Ba_xSr_{1-x}TiO_3$, and $SrTiO_3$, usually suffer from low breakdown strength and weak processability.[12,13] In contrast, polymers have many inherent advantages of high breakdown strength, low dielectric loss, easy-processing, and low cost.[14,15] Nevertheless, the low-k performance of polymers has hindered their wide utilization in dielectrics and energy storage devices. Thus, the introduction of high-k ceramic fillers into a polymer matrix has become a common approach to combine the merits of these two components. Much effort has been devoted to maximizing the dielectric constant, suppressing the dielectric loss, and maintaining the breakdown strength of polymer composites, which are all essential for the enhancement of the energy storage capability.[5,16−31] Ferroelectric polymers, such as poly(vinylidene fluoride) (PVDF) and its copolymer, have been widely used as a matrix because of their relatively high k.[14,15] Recent literature has demonstrated that the high-aspect-ratio ceramic fillers can enhance the dielectric constant of nanocomposites more efficiently than their corresponding spherical particles.[32−43] For example, Tang et al. reported that the dielectric constant of nanocomposites with 17.5 vol % loading of $BaTiO_3$ nanowires can reach up to 69.5, while that of nanocomposites with 30 vol % $BaTiO_3$ nanoparticles is just about 52, by using poly(vinylidene fluoride-trifluoroethylene-chlorofluoroethylene) (P(VDF-TrFE-CFE)) as the polymer matrix.[35] Furthermore, the energy storage density of the aforementioned nanocomposites is more than 45.3% higher than that of neat P(VDF-TrFE-CFE) under the electric field of 300 MV m^{-1}. Although the high-aspect-ratio nanowires exhibit superiority in enhancing k and the energy density of polymer nanocomposites, our understanding of the role of their intrinsic properties in determining the dielectric properties and energy storage of polymer nanocomposites is still poor.

Since the current research for high-k ceramic/polymer composites mostly encompasses either the introduction of single type inorganic ceramics or the promotion of the compatibility between ceramics and a polymer matrix, it is worthwhile to assess the influence of different kinds of nanofillers with different intrinsic properties on the dielectric properties of the subsequent proposed nanocomposites. Herein, we report the fabrication of the P(VDF-HFP)-based nanocomposites by using a series of surface modified nanowires. Nonferroelectric $Na_2Ti_3O_7$ and TiO_2, ferroelectric

Received: June 2, 2015
Accepted: July 30, 2015
Published: July 30, 2015

DOI: 10.1021/acsami.5b06480
ACS Appl. Mater. Interfaces 2015, 7, 18017−18027

$BaTiO_3$, and paraelectric $SrTiO_3$ NWs were synthesized respectively and then functionalized by dopamine. From the inherent property difference (such as crystallographic structure and dielectric constant) of these selected nanowires and the corresponding impact on the subsequent nanocomposites, we could learn about the potential of the tailoring electric properties of nanocomposites by adjusting the introduced nanofillers. The results and methods presented here provide deep insights into the design and fabrication of polymer nanocomposites for dielectric and energy storage applications.

EXPERIMENTAL SECTION

Materials. Titanium dioxide nanopowder (TiO_2, P25, ≥99.5%) was purchased from Sigma-Aldrich. Barium hydroxide octahydrate ($Ba(OH)_2{\cdot}8H_2O$, ACS, 98%), strontium hydroxide octahydrate ($Sr(OH)_2{\cdot}8H_2O$ ACS, 99.5%) and dopamine hydrochloride (98%) were supplied by Aladdin (China). Poly(vinylidene fluoride-*co*-hexafluoropylene) (P(VDF-HFP)) with 15% HFP was kindly provided by Solvay Plastics (Shanghai, China). Other chemicals or reagents were purchased from Sinopharm Chemical Reagent Co., Ltd. (China).

Synthesis of $Na_2Ti_3O_7$ Nanowires. The synthesis of $Na_2Ti_3O_7$ NWs was accomplished according to previous literature.[10,44,45] 3 g of titanium dioxide nanopowder was homogeneously dispersed in 60 mL of 10 M sodium hydroxide aqueous solution. The mixture was stirred for 12 h, and then transferred into a 90 mL Teflon-autoclave. The autoclave was subsequently stayed in an oven at 200 °C for 3 days. Then, the obtained $Na_2Ti_3O_7$ NWs were washed with deionized water and ethanol for several times. The pristine $Na_2Ti_3O_7$ NWs were collected after drying in a vacuum oven at 80 °C. In order to remove the crystal water, the pristine $Na_2Ti_3O_7$ NWs were further calcined in oven at 200 °C for another 4 h.

Synthesis of TiO_2 Nanowires. The TiO_2 NWs were synthesized from $Na_2Ti_3O_7$ NWs by a two-step method described in previous literature.[33] First, the synthesized pristine $Na_2Ti_3O_7$ NWs were soaked in a diluted 0.1 M hydrochloric acid aqueous solution for 24 h to get $H_2Ti_3O_7$ NWs. The obtained $H_2Ti_3O_7$ NWs were washed with deionized water and dried in vacuum at 80 °C. Next, the $H_2Ti_3O_7$ powder was put into an alumina crucible with a cover, then heated to 600 °C for 3 h with a heating rate of 20 °C min^{-1} to obtain TiO_2 NWs.

Synthesis of $BaTiO_3$ and $SrTiO_3$ Nanowires. The synthesis of $BaTiO_3$ and $SrTiO_3$ NWs were accomplished by adopting Tang's method.[34−36] Take the synthesis of $BaTiO_3$ NWs as example, 1.025 g $Ba(OH)_2{\cdot}8H_2O$ (3.25×10^{-3} mol) and 0.140 g $H_2Ti_3O_7$ (0.542×10^{-3} mol) were added into a 90 mL Teflon-autoclave and stirred for 24 h. Then, the autoclave was put into oven at 200 °C for 1.5 h. The obtained $BaTiO_3$ NWs were subsequently washed with diluted 0.1 M hydrochloric acid aqueous solution, deionized water, and ethanol for several times. The synthesis of $SrTiO_3$ NWs is similar to that of $BaTiO_3$ NWs, by replacing $Ba(OH)_2{\cdot}8H_2O$ with $Sr(OH)_2{\cdot}8H_2O$ while keeping the other process same.

Surface Modification of Nanowires. In a typical process, the nanowires were dispersed into an aqueous solution of dopamine hydrochloride with a concentration of 2 g L^{-1} under stirring for 24 h at 60 °C. The pH of the dopamine solution was buffered to 8.5 by adding 10 mM Tris-HCl. With the spontaneous deposition of adherent polydopamine film on the surface of nanowires, the color of the mixture was finally changed to dark brown. Those functionalized nanowires were named as dopa@$Na_2Ti_3O_7$, dopa@TiO_2, dopa@$BaTiO_3$ and dopa@$SrTiO_3$, respectively.

Fabrication of P(VDF-HFP)-Based Nanocomposite Films. The typical process for the fabrication of P(VDF-HFP)-based nanocomposites films was carried out as follows: P(VDF-HFP) was first dissolved in DMF and stirred overnight to get a homogeneous solution. Meanwhile, the proposed nanowires were ground thoroughly and dispersed in DMF by ultrasonication for 1 h, which were subsequently mixed in the required volume ratio with P(VDF-HFP) solution. Then, the mixture was stirred vigorously for 24 h. Before casting on a glass plate, the dispersion was first ultrasonicated with piezoelectric vibrator for 5 min. The cast films were dried at 90 °C for 2 h. Subsequently, the films were peeled off the glass substrate and dried at 90 °C for another 12 h in a vacuum oven to remove the remaining trace solvent. Finally, the nanocomposites were compressed into thin films by hot-pressing at 190 °C with a pressure of about 20 MPa. Nanocomposites containing different volume fractions (2.5%, 5%, 7.5%, and 10%) of dopamine modified nanowires ($Na_2Ti_3O_7$, TiO_2, $BaTiO_3$, and $SrTiO_3$) were prepared, respectively. The typical thickness of P(VDF-HFP)-based nanocomposites films was around 50 μm.

Characterization. Characterization of the morphology of the nanowires and samples was performed by SEM (Nova NanoSEM 450, FEI, USA) and TEM (JEM-2010, JEOL, Japan). The cross-section SEM images of nanocomposites films were prepared by fracturing the films in liquid nitrogen. The samples for the TEM were prepared by dropping a few drops of the sample solution on a carbon-coated cooper grids and air-dried before measurement. The crystalline structure of the nanowires were determined by X-ray diffractometer (D/max-2200/PC, Rigaku, Japan) with Cu Kα source. The chemical structures of the pristine and surface modified nanowires were characterized by the Fourier-transform infrared spectroscopy (FT-IR) over the range of 4000−400 cm^{-1} with a PerkinElmer Paragon 1000 spectrometer. X-ray photoelectron spectra (XPS) of the nanowires were conducted using an Axis UltraDLD spectrometer (Shimadzu-Kratos Analytical, UK) with a monochromated Al Kα source. Thermogravimetric analysis (TGA) of nanowires was performed using NETZSCH TG209 F3 with a heating rate of 20 °C min^{-1} in a nitrogen flow (20 mL min^{-1}). Differential scanning calorimetry (DSC) characterization of the nanocomposites was conducted under nitrogen atmosphere at a heating/cooling rate of 10 °C min^{-1} with the range of 20 to 200 °C by using a NETZSCH 200 F3 instrument. The dielectric properties of the samples were measured by using a Novocontrol Alpha-N high resolution dielectric analyzer (GmbH Concept 40) with the frequency range 10^{-1}−10^6 Hz at room temperature. A layer of gold was evaporated on both sides of the samples to serve as electrodes. The DC breakdown strength was measured by using a dielectric strength tester with a ball to ball stainless electrode (DH, Shanghai Lanpotronics Co., China). All the samples used for breakdown strength have a thickness of around 60 μm. Electric displacement-electric field (D−E) loops and two probe current−voltage (I−V) measurements were conducted by a Precision Multiferroic Materials Analyzer equipped with Precision 10 kV HVI-SC and Trek MODEL 609B (Radiant Inc.). Samples were sputtered by gold with diameter of 3 mm on both sides as electrodes.

RESULTS AND DISCUSSION

Preparation and Characterization of the Pristine and Surface Modified Nanowires. Figure 1 depicts the crystal structures of the utilized $Na_2Ti_3O_7$, TiO_2 (anatase), $BaTiO_3$, and $SrTiO_3$, respectively. As shown in Figure 1a and Figure S1 (Supporting Information), for $Na_2Ti_3O_7$, three edge sharing TiO_6 octahedrons are arranged in a zigzag pattern and sodium ions are inserted among the TiO_6 layers. The layered titanate structure, maintained by sodium ions under hydrothermal treatment at high temperature, provides the space for sodium ions to diffuse or transport easily, which facilitates the further synthesis of subsequent nanowires. Except for the distinctive loose crystallographic structure of $Na_2Ti_3O_7$, the other three types of ceramic nanofillers possess the condensed structure (Figure 1b−1d). Figure 2a shows the free-standing $Na_2Ti_3O_7$ NWs. In order to eliminate the influence of crystal water inside the pristine $Na_2Ti_3O_7$ NWs on the following fabrication of nanocomposites, the calcination at 200 °C was adopted. As shown in Figure S4a (Supporting Information), the calcined $Na_2Ti_3O_7$ NWs are about several micrometers in length and

DOI: 10.1021/acsami.5b06480
ACS Appl. Mater. Interfaces 2015, 7, 18017−18027

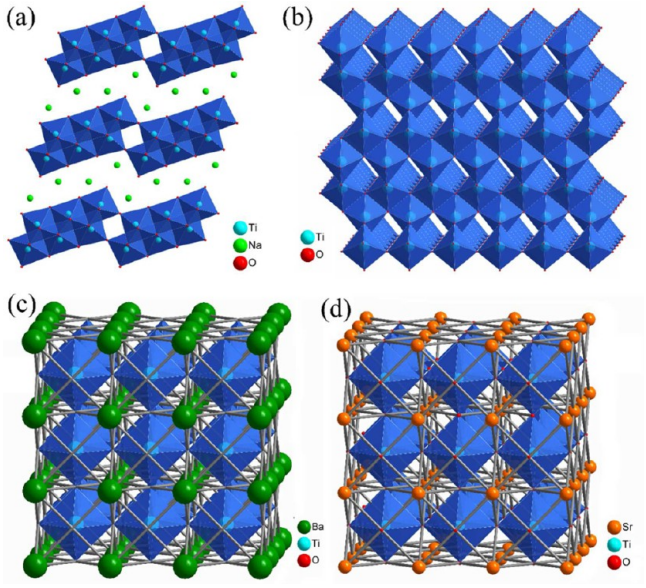

Figure 1. Crystal structures of (a) $Na_2Ti_3O_7$, (b) anatase TiO_2, (c) $BaTiO_3$, and (d) $SrTiO_3$ with TiO_6 polyhedron.

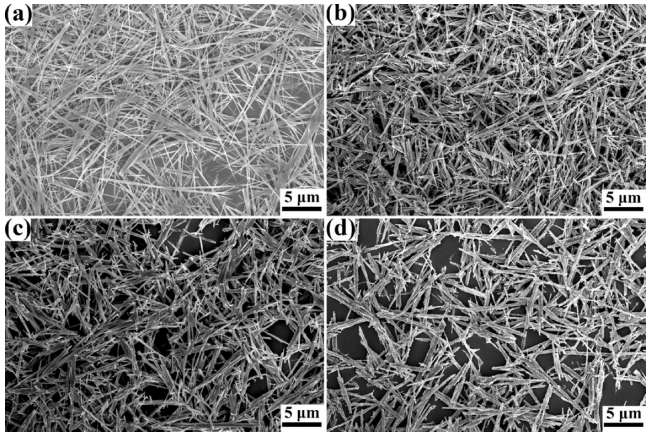

Figure 2. SEM images of (a) $Na_2Ti_3O_7$, (b) TiO_2, (c) $BaTiO_3$, and (d) $SrTiO_3$ NWs.

retain the morphology of the original nanowires. The TiO_2 NWs were generated through the high-temperature annealing of $H_2Ti_3O_7$ NWs (Figure S4b, Supporting Information). As shown in Figure 2b, the morphology of TiO_2 NWs is similar to that of the as-synthesized $H_2Ti_3O_7$ NWs, even after the calcination and dehydration. The two-step hydrothermal reaction is employed to give $BaTiO_3$ and $SrTiO_3$ NWs. The introduction of barium or strontium made the original $H_2Ti_3O_7$ NWs rougher, which was consistent with the results of previous literature.[34−36] The successful injection of barium or strontium ions to the $H_2Ti_3O_7$ NWs was guaranteed by the high temperature (200 °C), while the morphology change was prevented efficiently within a relatively short time (1.5 h), as the structure collapse and recrystallization of $H_2Ti_3O_7$ with open structure were minimized.[46] The successful synthesis of four kinds of nanowires is further evidenced by the X-ray diffraction (XRD) patterns (Figure S5, Supporting Information).

In order to improve the compatibility between the nanowires and polymer matrix, these kinds of nanowires were functionalized with dopamine. The deposition of polydopamine can give a distinct thin layer on the nanowire surface, which facilitates the dispersion of nanowires in the polymer matrix. Figure S6 (Supporting Information) presents the transmission electron microscopy (TEM) images of the pristine nanowires (top row) and surface modified nanowires (bottom row). After the surface modification, an amorphous layer of several nanometers thickness can be clearly observed on the nanowire surface. The Fourier transform infrared spectroscopy (FT-IR) and X-ray photoelectron spectroscopy (XPS) are further used to validate the successful coating of the polydopamine layer on the surface of the nanowires. As shown in the FT-IR spectra in Figure S7 (Supporting Information), obvious changes between 1600 and 1300 cm^{-1} can be observed after the dopamine functionalization, which are ascribed to the specific N−H bending vibrations and aromatic amine C−N stretching vibrations in the dopamine.[41] Furthermore, the presence of the N 1s peak at a binding energy of 400 eV in the XPS spectra also confirmed that the nitrogen-containing dopamine had been adhered on the nanowire surface through the oxidative self-polymerization of dopamine (Figure S8, Supporting Information).[41−43,47]

Thermogravimetric analysis (TGA) was employed to investigate the difference of composition and thermal stability between the pristine and surface modified nanowires. As shown in Figure S9a (Supporting Information), the total weight loss of the pristine $Na_2Ti_3O_7$ from 50 to 800 °C was about 10.11 wt %, while the main weight loss occurred below 200 °C. The loss was then notably reduced to 3.19 wt % after the calcination at 200 °C for several hours. However, the dehydration of $Na_2Ti_3O_7$ may give rise to the formation of voids, which was a benefit for the subsequent functionalization and deposition of dopamine. This hypothesis was further evidenced by the remarkable weight loss of dopa@$Na_2Ti_3O_7$ (11.15 wt %). For the other three kinds of nanowires, the increase of weight loss after functionalization should be attributed to the coating of polydopamine on the nanowire surface (Figure S9b−S9d, Supporting Information).

Microstructure of P(VDF-HFP)-Based Nanocomposites. P(VDF-HFP)-based nanocomposite films with given volume fractions (2.5%, 5%, 7.5%, and 10%) of different nanowires were fabricated by solution blending. Figure 3 presents the SEM images of freeze-fractured cross-sectional

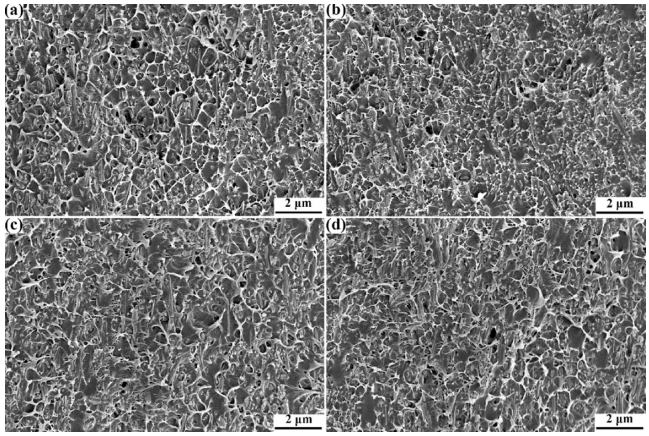

Figure 3. SEM images of freeze-fractured cross-sectional surfaces of P(VDF-HFP)-based nanocomposites with 10 vol % loading of dopamine modified (a) $Na_2Ti_3O_7$, (b) TiO_2, (c) $BaTiO_3$, and (d) $SrTiO_3$ NWs.

DOI: 10.1021/acsami.5b06480
ACS Appl. Mater. Interfaces 2015, 7, 18017−18027

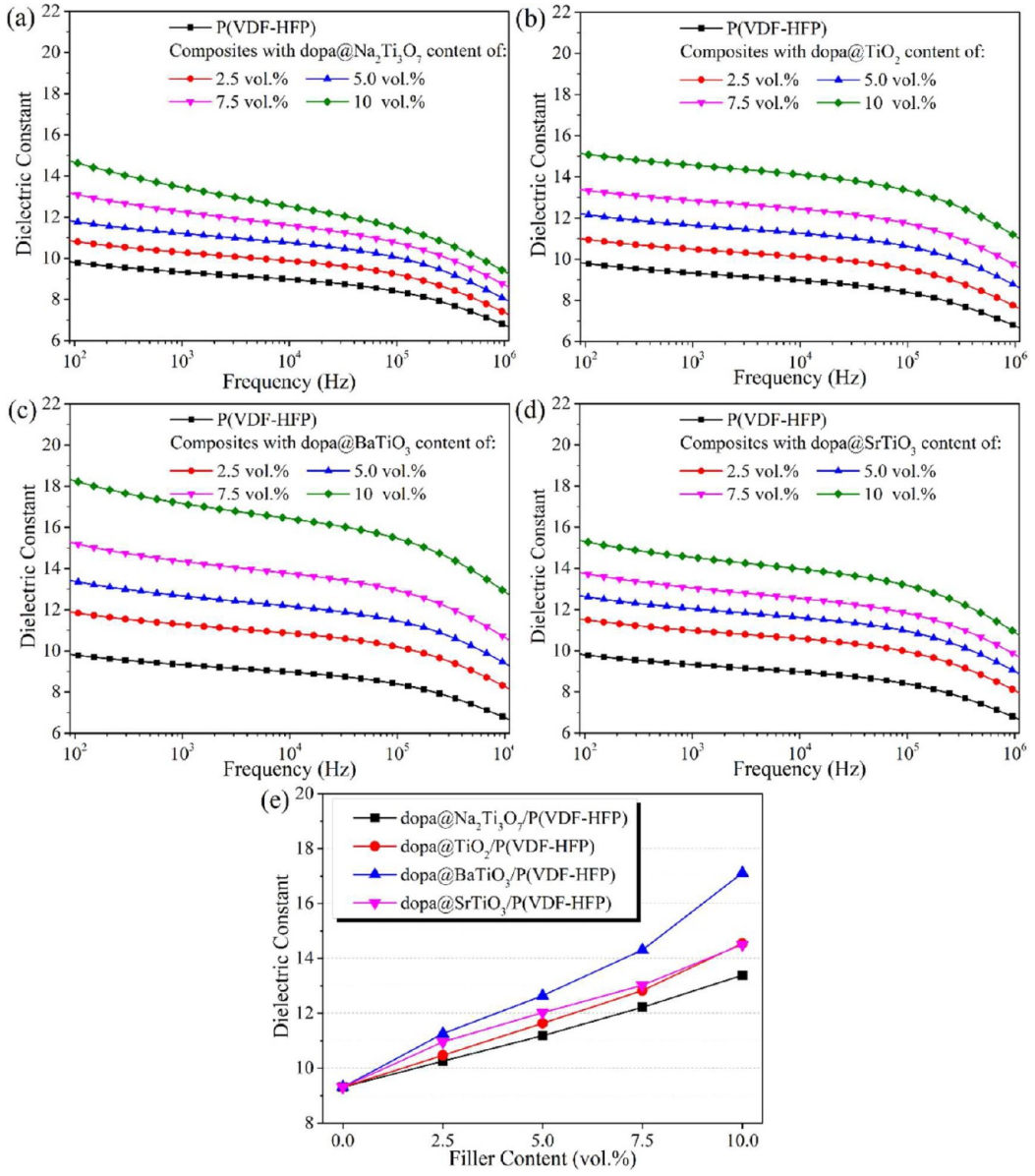

Figure 4. (a–d) Dielectric constant of P(VDF-HFP)-based nanocomposites with different volume fractions of nanowires versus the frequency. (e) Dielectric constant of P(VDF-HFP)-based nanocomposites with different volume fractions of nanowires at 1 kHz.

surfaces of the nanocomposites with 10 vol % nanowires. As shown in Figure 3, the polydopamine coated nanowire surface are homogeneously distributed in the polymer matrix. We could observe that those nanowires are buried well inside the polymer matrix, and no tail of those nanowires is found to stretch outside the cross-section surfaces. Those discrete holes on the cross section may originate from the freeze-fracture process of the samples for SEM investigation. The breakage of nanowires implies their excellent interfacial bonding with the polymer matrix as the nanowires are tightly held in the matrix. Such microstructure characteristics of the nanocomposites indicate that the polydopamine coated nanowires exhibit excellent compatibility with the P(VDF-HFP) matrix.

Dielectric Properties of the P(VDF-HFP)-Based Nanocomposites. The traditional approach of high-*k* nanocomposites *via* introducing high volume fraction (usually about 40%) of high-*k* nanofillers into polymer matrix usually causes significant decrease of breakdown strength of the proposed nanocomposites.[32,48,49] Herein, in order to maintain the high breakdown strength of polymer matrix, the highest fraction of nanowires is set to 10 vol %. Within this small loading, the composite films are still highly flexible for further processing and practical applications. The enhanced dielectric constants of nanowire fillers over the polymer matrix are shown in Figure 4. The dielectric constants of the nanocomposites witness a gradual increase with the loading of nanowires, while the dielectric loss remains basically unchanged in comparison to the pure P(VDF-HFP) (Figure S11, Supporting Information). The increase in dielectric constants of the nanocomposites originates from the electric field enhancement in the polymer matrix induced by the high-*k* nanowires. As the intrinsic dielectric constants of these inorganic nanowires are much larger than that of P(VDF-HFP) matrix, the dielectric constant enhancement can be more significant as the volume fraction increases, resulting in the apparent enhancement of dielectric constants of nanocomposites with high nanowire loadings. From Figure 4, we could also find that the dielectric constants of polymer matrix and nanocomposites gradually decrease with

DOI: 10.1021/acsami.5b06480
ACS Appl. Mater. Interfaces 2015, 7, 18017–18027

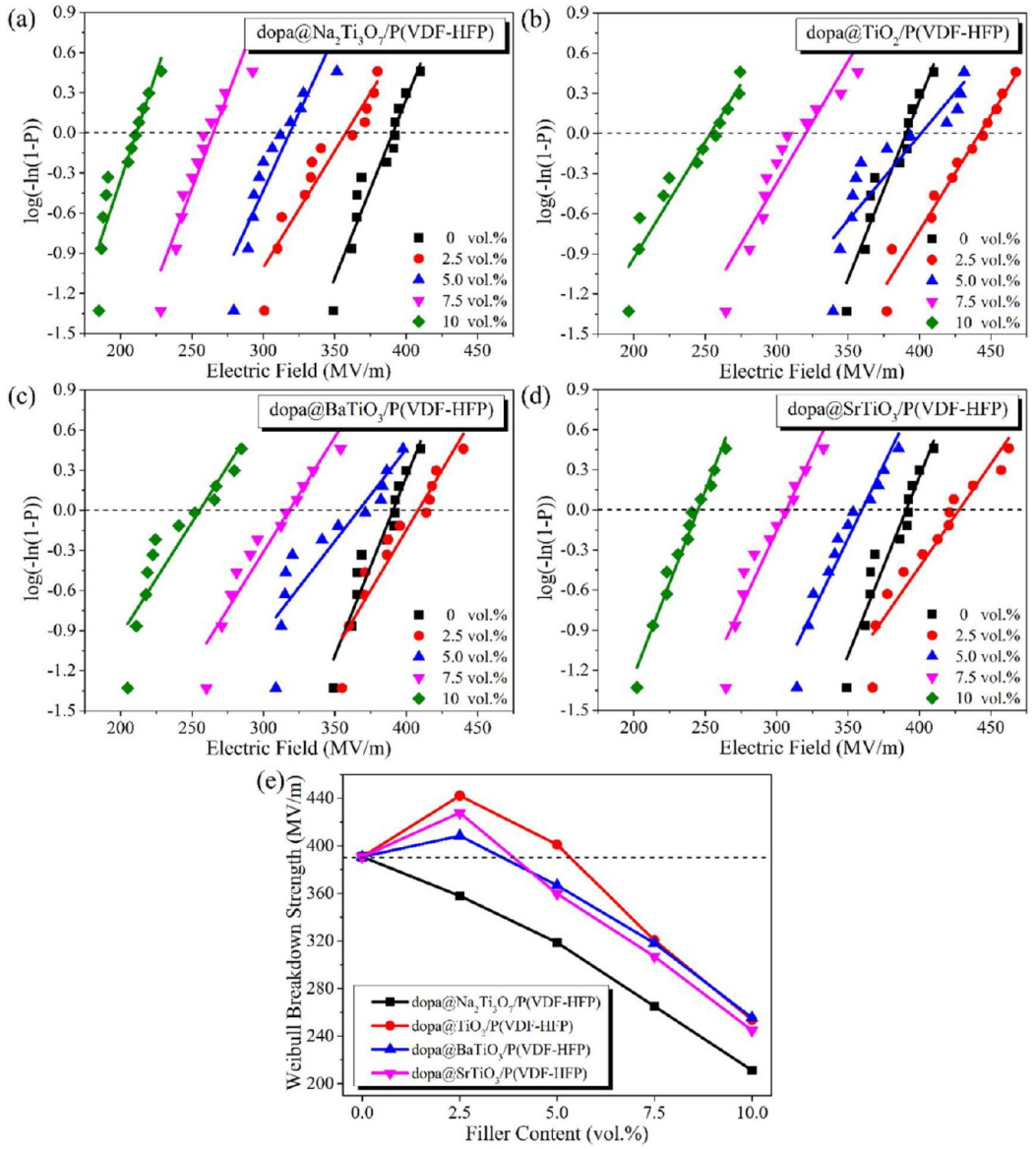

Figure 5. (a–d) Weibull plots for P(VDF-HFP)-based nanocomposites with different volumes fractions of nanowires. (e) Weibull breakdown strength of the P(VDF-HFP)-based nanocomposites at varied volume fractions of nanowires.

the increase of frequency. This behavior can be attributed to the restricted dipole mobility of the polymer matrix and the decreased strength of slow polarization (i.e., interfacial polarization) at high frequencies.[26,50,51] The interfacial polarization increases with the growth of nanowire/polymer interfacial area, resulting in strong frequency dependent dielectric constant in nanocomposites with high loading of nanowires, particularly at low frequencies. As shown in Figure S11 (Supporting Information), the nanocomposites show comparable or slightly enhanced dielectric loss tangent in comparison with the pure polymer, which might be ascribed to the good interface compatibility between the dopamine modified nanowires and the polymer matrix.

Figure 4e represents the dielectric constants of those nanocomposites at 1 kHz. The dielectric constant of the nanocomposite containing 10 vol % dopa@$BaTiO_3$ is nearly doubled in comparison with that of pure P(VDF-HFP). Among those four kinds of nanowires, the introduction of dopa@$Na_2Ti_3O_7$ brings the gentlest enhancement of dielectric constant, which may originate from the smallest intrinsic dielectric constant of $Na_2Ti_3O_7$. From Figure 4, we can clearly observe that the intrinsic properties of the introduced nanowires did have an apparent effect on the dielectric properties of the proposed nanocomposites. Among those four kinds of nanowires, $BaTiO_3$ is the best candidate for the preparation of high-k nanocomposites from the dielectric property perspective.

Breakdown Strength and Energy Storage of P(VDF-HFP)-Based Nanocomposites. Breakdown strength (E_b) is an important parameter for the practical applications as it determines the operation electric field and the maximum energy storage density of dielectric materials. The characteristic E_b of the P(VDF-HFP)-based nanocomposites with different volume fractions and different kinds of nanowire fillers is analyzed using a two-parameter Weibull statistic distribution method eq 1,[52]

$$P(E) = 1 - \exp[-(E/E_0)^{\beta}] \quad (1)$$

DOI: 10.1021/acsami.5b06480
ACS Appl. Mater. Interfaces 2015, 7, 18017–18027

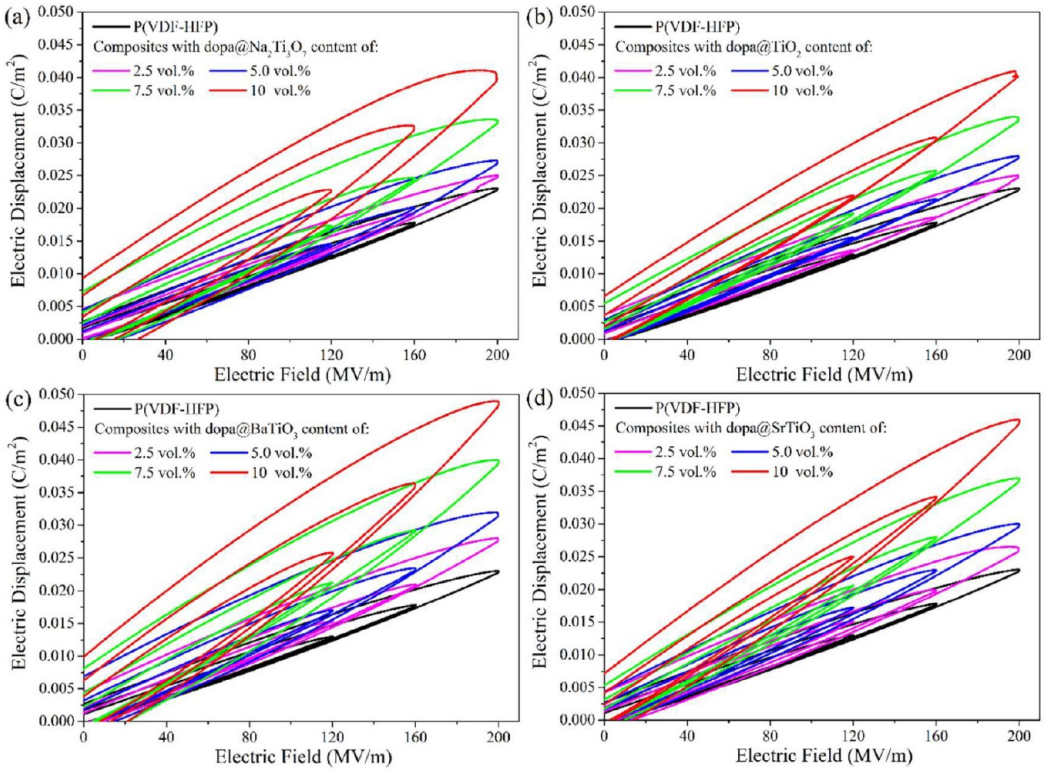

Figure 6. Electric displacement–electric field (D–E) loops of P(VDF-HFP)-based nanocomposites with different volume fractions of nanowires under different applied fields at room temperature: (a) dopa@$Na_2Ti_3O_7$/P(VDF-HFP), (b) dopa@TiO_2/P(VDF-HFP), (c) dopa@$BaTiO_3$/P(VDF-HFP), and (d) dopa@$SrTiO_3$/P(VDF-HFP).

where $P(E)$ is the cumulative probability of electrical failure, E is an experimental breakdown strength, β is the shape parameter which is related to the scatter of the data and a higher value of it represents higher level of dielectric reliability, E_0 is the characteristic breakdown that represents the breakdown strength at the cumulative failure probability of 63.2%. E_0 is the scale parameter to compare the differences in breakdown strength among different specimens. Herein, the breakdown strength is extracted from a fit using Weibull failure statistics across 12 specimens per sample.

Figure 5 shows the characteristic breakdown strength of P(VDF-HFP)-based nanocomposites with the different volume fractions of nanowires. As summarized in Figure 5e, E_b is enhanced upon the incorporation of 2.5 vol % nanowires, from the 391 MV m^{-1} for the pristine P(VDF-HFP) to 442 MV m^{-1}, 408 MV m^{-1}, and 428 MV m^{-1} for the nanocomposites with dopa@TiO_2, dopa@$BaTiO_3$ and dopa@$SrTiO_3$ NWs, respectively. However, it should be noticed that the breakdown strength of nanocomposites with dopa@$Na_2Ti_3O_7$ is gradually decreased, accompanied by the increased nanowire loading. The breakdown strength increase of the nanocomposites at low loading of nanofillers is consistent with some previous literature.[41−43,53−55] Compared with the pure polymer, the enhanced breakdown strength of nanocomposites with dopa@TiO_2, dopa@$BaTiO_3$ and dopa@$SrTiO_3$ NWs may be attributed to the following reasons: (i) The highly ordered and dense architecture of the three nanowires (Figure 1) makes them highly insulating, resulting in weak increase of leakage current density in the nanocomposites; (ii) The high-aspect-ratio nanowires tend to orient toward the in-plane directions during the solution-cast process of the nanocomposite films, as demonstrated by previous studies, resulting in anisotropic polymer nanocomposite dielectrics.[39,40,54−56] These nanowires may give rise to anisotropy in the susceptibility of the nanocomposite films under the applied electric field in the out-of-plane directions, resulting in a lower concentration of electric field in the polymer matrix.[41−43] Besides, the oriented nanowires in the nanocomposites may restrain the growth of electrical treeing by bringing up twisted pathways for treeing and acting as scattering centers for the charge carriers within the nanocomposites.[41−43]

However, as shown in Figure 5e, the introduction of nanowires results in a decrease of breakdown strength at higher nanowire loading (≥5.0 vol %). The decrease trend becomes more significant with further increase of nanowire loading. This observation could be attributed to remarkable enhancement of electric field upon the polymer matrix, caused by large electrical mismatch between nanowire and the polymer. The breakdown strength of dopa@TiO_2/P(VDF-HFP) seems to be superior to that of nanocomposites with the other three nanowires. This phenomenon can be understood by the fact that TiO_2 nanowires and polymer matrix possess the comparable dielectric constant, which can effectively minimize the field distortion within the polymer matrix.[5,57,58] At the highest loading of 10 vol % nanowires, the breakdown strength of the nanocomposites is all in the range of 210 MV m^{-1} to 260 MV m^{-1}, which is still high enough for practical applications. High breakdown strength is definitely the prerequisite to the dielectric materials for energy storage applications, as the theoretical maximum energy storage density of a liner response dielectric material can be defined by the eq 2,[4]

$$U_e = 1/2\varepsilon_r\varepsilon_0 E_b^2 \quad (2)$$

DOI: 10.1021/acsami.5b06480
ACS Appl. Mater. Interfaces 2015, 7, 18017−18027

where ε_r is the relative dielectric constant, ε_0 the vacuum permittivity (8.8542×10^{-12} F m^{-1}), and E_b the dielectric breakdown strength. The calculated maximum energy storage densities of the nanocomposites are shown in the Figure S12 (Supporting Information). Obviously, all the nanocomposites exhibit a peak maximum energy storage density at 2.5 vol % nanowire loading. Starting from 5 vol % nanowire loading, the maximum energy storage densities of nanocomposite decrease with the increase of the nanowire loading because of the large decrease of breakdown strength. When the nanowire loading reaches 10 vol %, all the nanocomposites exhibit lower maximum energy storage densities compared with the pure polymer. These results indicate that a small loading of suitable nanofillers is more effective to enhance the energy storage capability of polymers.

For ferroelectric materials, the polarization of the materials is not linear dependent on the applied electric field. Thus, the energy density is also related to the polarization with respect to the applied electric field. Generally, the Sawyer−Tower circuit is employed to determine the relationship between the polarization and electric field. On the basis of this approach, the energy storage capability of the dielectric materials can be evaluated from the D−E loops based on the following integral eq 3,

$$U_e = \int E dD \tag{3}$$

where E is the electric field, and D is the electric displacement.

The D-E loops measured at 100 Hz with varying electric field for the nanocomposite films with different loading of nanowires are presented in Figure 6. It can be observed that the electric displacement of the nanocomposites increases with the volume fractions of nanofillers, resulting from the higher dielectric constants of the nanowires in comparsion with the polymer matirx (Table S1, Supporting Information). Also, at the same loading, the introduction of $BaTiO_3$ gives the most signficant enhancement for electric displacement of the nanocomposites, followed by $SrTiO_3$, TiO_2, and $Na_2Ti_3O_7$, respectively. This trend is actually consistent with the dielectric constant comparsion of these nanofillers. Namely, the electric displacement enhancement of nanocomposites would become more remarkable if the nanofiller with higher k were introduced. The total stored and discharged energy densities at 200 MV m^{-1} calculated from eq 4 are summarized in Figure 7a and 7b. Obviously, both the total stored and discharged energy densities increase with the volume fractions of nanowire fillers. Among these four kinds of functionalized nanowires, dopa@$BaTiO_3$ NWs are demonstrated to be the best fillers, as the energy densities of which are superior the others, followed by dopa@$SrTiO_3$ NWs. From Figure 7a, we can observe that the total stored energy density of the nanocomposite with 10 vol % dopa@$BaTiO_3$ are 5.91 J cm^{-3}, more than twice of the pristine P(VDF-HFP) polymer (2.54 J cm^{-3}). Meanwhile, the discharged energy density of the nanocomposite with 10 vol % dopa@$BaTiO_3$ is also increased up to 3.37 J cm^{-3}, while the value of pristine polymer is only 1.85 J cm^{-3} (Figure 7b). Compared with the nanocomposites with dopa@$Na_2Ti_3O_7$, the nanocomposites with dopa@TiO_2 exhibit higher discharged energy densities, which are more important for the practical applications.

The energy storage efficiency (η) is another important parameter for the evaluation of energy-storage materials for practical applications. Low energy storage efficiency can lead to the heating and aging of the components, which have adverse effects on the reliability and performance of the materials. Therefore, it is necessary to fabricate the nanocomposites with high energy storage efficiency. Figure 7c shows the efficiency of nanocomposites with increased loading of nanowires. Due to the larger hysteresis in the polarization caused by increased loading of nanowires, the efficiency decreases just as predicted. Interesting, the nanocomposites with dopa@TiO_2 show superior efficiency than those of the nanocomposites with other kinds of nanowires. This improved efficiency could be attributed to the smaller remanent polarization of the dopa@TiO_2 NWs filled nanocomposites, as shown in Figure 6. Besides, the efficiency downtrend of dopa@$SrTiO_3$/P(VDF-HFP) is somewhat more gradual than that of dopa@$BaTiO_3$/P(VDF-HFP), resulting from the paraelectric phase and little hysteresis behavior of $SrTiO_3$.[34,37,59] At the 10 vol % loading,

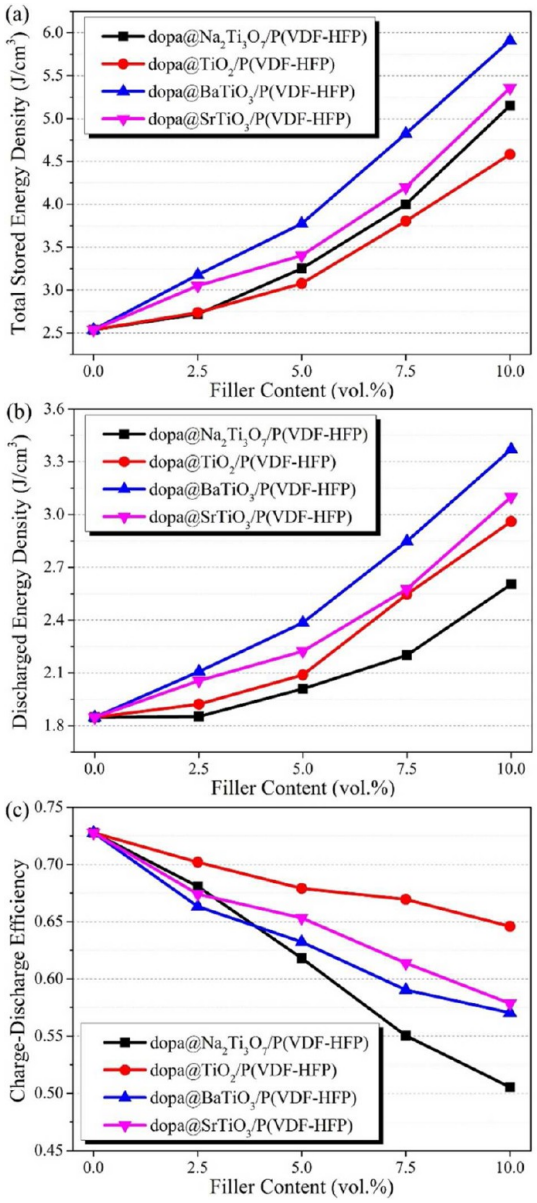

Figure 7. Total storage energy density (a), discharged energy density (b), and charge−discharge efficiency (c) of P(VDF-HFP)-based nanocomposites versus the volume fractions of dopamine modified nanowires.

DOI: 10.1021/acsami.5b06480
ACS Appl. Mater. Interfaces 2015, 7, 18017−18027

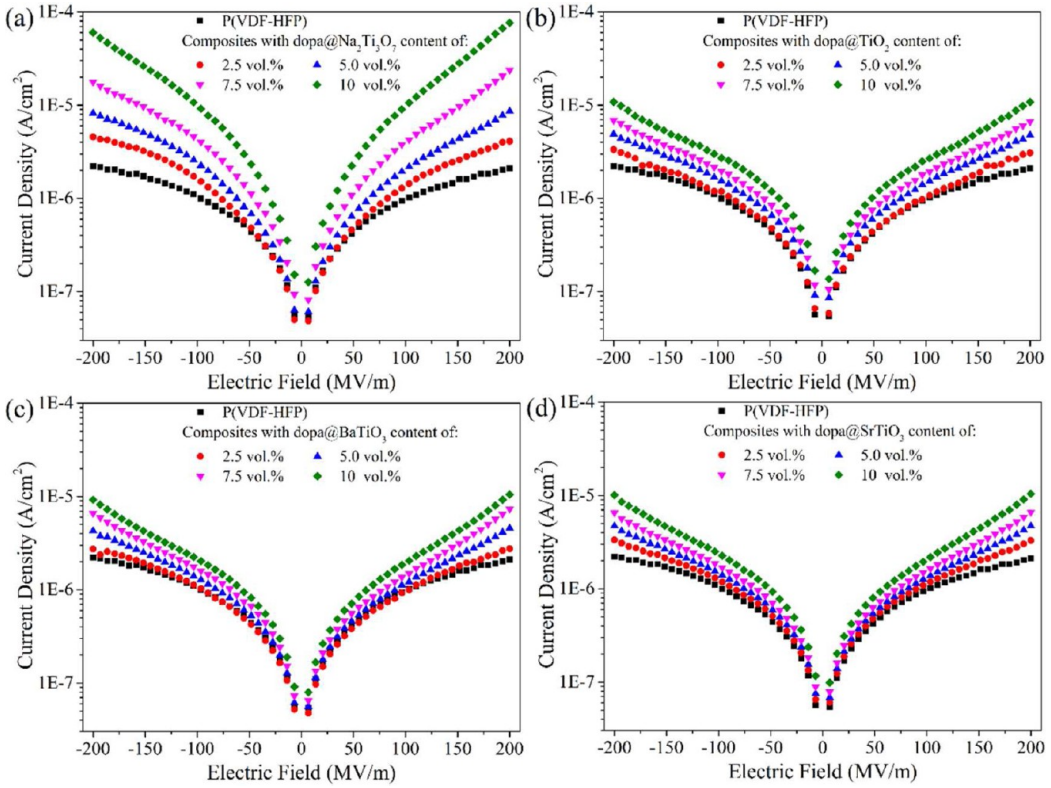

Figure 8. Leakage current density of P(VDF-HFP)-based nanocomposites with different volume fractions of nanowires at varied applied electric field: (a) dopa@$Na_2Ti_3O_7$/P(VDF-HFP), (b) dopa@TiO_2/P(VDF-HFP), (c) dopa@$BaTiO_3$/P(VDF-HFP), and (d) dopa@$SrTiO_3$/P(VDF-HFP). Inset: Leakage current density of P(VDF-HFP)-based nanocomposites with different loading of each nanowire at the applied electric field 200 MV m^{-1}.

the efficiencies of the nanocomposites with dopa@$BaTiO_3$ and dopa@$SrTiO_3$ are both reduced to around 57%, which are about 16% lower than that of the pristine polymer matrix. At higher nanowire loading, dopa@$Na_2Ti_3O_7$/P(VDF-HFP) nanocomposites exhibit the lowest energy storage efficiency because of their high remanent polarization (Figure 6) and large leakage current densities of the nanocomposites (shown below). These results indicate that the modulation of energy storage capability of the nanocomposites can be realized by adopting the nanofillers with different intrinsic properties.

Leakage Current Density of P(VDF-HFP)-Based Nanocomposites. The leakage current densities of the present nanocomposite films are shown in Figure 8. Expect for dopa@$Na_2Ti_3O_7$/P(VDF-HFP), of which the maximum leakage current densities have been approximated to 10^{-4} A cm^{-2} at the applied electric field of 200 MV m^{-1}, the leakage current densities of the nanocomposites with the other nanowires are all lied in the range of 10^{-8} to 10^{-5} A cm^{-2}. The leakage current densities follow a reasonable increase trend with the raise of applied electric field. For each kind of nanowire fillers, the nanocomposites exhibit gradually increased leakage current densities with the loading of the nanowires, originating from the defects and space charge introduced by the nanowire inclusions. The leakage current densities of the present nanocomposites versus the volume fractions of nanowires have been summarized in Figure S13 (Supporting Information). At the applied electric field of 200 MV m^{-1}, the nanocomposite with 10 vol % dopa@$Na_2Ti_3O_7$ loading shows a significant increase in the leakage current density when compared with the pristine polymer matrix, which did have an obvious influence on the aforementioned properties. Nonetheless, for the other nanowires at the same loading, the leakage current densities for the nanocomposites are all around 10^{-5} A·cm^{-2}. The resistivity of these nanocomposites with the loading functionalized nanowires calculated from the I–V characteristics are 10^{10}–10^{12} Ω·cm. Namely, the proposed nanocomposites are excellent insulating materials qualified for the practical applications. But the poor performance of the nanocomposites with dopa@$Na_2Ti_3O_7$ NWs indicates that the $Na_2Ti_3O_7$ might be an inappropriate choice in the construction of nanocomposites for dielectric related and energy storage applications.

CONCLUSIONS

In conclusion, we have successfully fabricated novel high-*k* nanocomposites composed of ferroelectric P(VDF-HFP) and a series of nanowires with different intrinsic properties. The homogeneous dispersion of these nanowires in the polymer matrix is realized by the deposition and coating of a thin polydopamine layer on their surface. The dielectric constants are greatly increased with the loading of those modified nanowires in comparison with the pristine polymer matrix, while the dielectric loss is still kept similar to that of neat P(VDF-HFP). For instance, at 1 kHz, the dielectric constant of the nanocomposite containing 10 vol % dopa@$BaTiO_3$ NWs is nearly doubled when compared with that of a pure P(VDF-HFP) matrix. The breakdown strengths of these proposed nanocomposites show a modest increase at a small loading of 2.5 vol %, except dopa@$Na_2Ti_3O_7$. Further decrease of the breakdown strength can be observed because of the defect introduced by the increased nanowire loading. Despite that, the

DOI: 10.1021/acsami.5b06480
ACS Appl. Mater. Interfaces 2015, 7, 18017–18027

proposed nanocomposites can still withstand over the electric field of 200 MV m^{-1}. Moreover, substantial enhancements in electric displacement and energy density at high electric fields have been demonstrated in the proposed nanocomposites. Taking the nanocomposite with 10 vol % dopa@$BaTiO_3$ loading as an example, the discharged energy density is significantly increased to 3.37 J cm^{-3}, while that of pristine polymer is only 1.85 J cm^{-3}. Dopa@$Na_2Ti_3O_7$/P(VDF-HFP) nanocomposites possess the worst performance owing to their high remanent polarization and large leakage current densities. Among the four types of nanowires, dopa@$BaTiO_3$ NWs are demonstrated to be the best candidates for potential dielectric and energy storage applications. These results demonstrate that the different inherent characteristics of the nanowires have an unambiguous effect on the electric properties (dielectric performance, breakdown strength, energy storage capability, and leakage current densities) of the subsequent proposed nanocomposites. Furthermore, we could learn about the potential of the tailoring electric properties of nanocomposites by adjusting the introduced nanofillers. Overall, this work provides deep insights into the influence of the nanofillers on the dielectric performance and energy storage capability of polymer composites. Besides, the results also pave the way for the further performance control of high-*k* nanocomposites.

■ ASSOCIATED CONTENT

Supporting Information

The Supporting Information is available free of charge on the ACS Publications website at DOI: 10.1021/acsami.5b06480.

Additional crystal structures, SEM images, TEM images, FT-IR spectra, DSC curves, and other figures and tables (PDF)

■ AUTHOR INFORMATION

Corresponding Author

* E-mail: xyhuang@sjtu.edu.cn (X.Y.H.).

Notes

The authors declare no competing financial interest.

■ ACKNOWLEDGMENTS

The financial support from the National Natural Science Foundation of China (nos. 51277117, 51477096) and the Special Fund of the National Priority Basic Research of China under Grant 2014CB239503 is gratefully acknowledged. Xingyi Huang acknowledges the 2013 SMC Excellent Young Faculty Award of Shanghai Jiao Tong University and Shanghai Pujiang Program under Grant PJ14D018. The authors are also grateful to researchers in the Instrument Analysis Center of Shanghai Jiao Tong University for their help with XPS measurements using an Axis UltraDLD spectrometer (Shimadzu-Kratos Analytical Ltd, UK) for materials analysis.

■ REFERENCES

(1) Li, Q.; Han, K.; Gadinski, M. R.; Zhang, G.; Wang, Q. High Energy and Power Density Capacitors from Solution-Processed Ternary Ferroelectric Polymer Nanocomposites. *Adv. Mater.* **2014**, *26*, 6244−6249.

(2) Hardy, C. G.; Islam, M. S.; Gonzalez-Delozier, D.; Morgan, J. E.; Cash, B.; Benicewicz, B. C.; Ploehn, H. J.; Tang, C. Converting an Electrical Insulator into a Dielectric Capacitor: End-Capping Polystyrene with Oligoaniline. *Chem. Mater.* **2013**, *25*, 799−807.

(3) Zhang, Q. M.; Li, H.; Poh, M.; Xia, F.; Cheng, Z. Y.; Xu, H.; Huang, C. An All-Organic Composite Actuator Material with a High Dielectric Constant. *Nature* **2002**, *419*, 284−287.

(4) Chu, B.; Zhou, X.; Ren, K.; Neese, B.; Lin, M.; Wang, Q.; Bauer, F.; Zhang, Q. M. A Dielectric Polymer with High Electric Energy Density and Fast Discharge Speed. *Science* **2006**, *313*, 334−336.

(5) Dang, Z.-M.; Yuan, J.-K.; Yao, S.-H.; Liao, R.-J. Flexible Nanodielectric Materials with High Permittivity for Power Energy Storage. *Adv. Mater.* **2013**, *25*, 6334−6365.

(6) Ortiz, R. P.; Facchetti, A.; Marks, T. J. High-*k* Organic, Inorganic, and Hybrid Dielectrics for Low-Voltage Organic Field-Effect Transistors. *Chem. Rev.* **2010**, *110*, 205−239.

(7) Salemizadeh Parizi, S.; Mellinger, A.; Caruntu, G. Ferroelectric Barium Titanate Nanocubes as Capacitive Building Blocks for Energy Storage Applications. *ACS Appl. Mater. Interfaces* **2014**, *6*, 17506−17517.

(8) Paniagua, S. A.; Kim, Y.; Henry, K.; Kumar, R.; Perry, J. W.; Marder, S. R. Surface-Initiated Polymerization from Barium Titanate Nanoparticles for Hybrid Dielectric Capacitors. *ACS Appl. Mater. Interfaces* **2014**, *6*, 3477−3482.

(9) Baeg, K.-J.; Khim, D.; Kim, J.; Han, H.; Jung, S.-W.; Kim, T.-W.; Kang, M.; Facchetti, A.; Hong, S.-K.; Kim, D.-Y.; Noh, Y.-Y. Controlled Charge Transport by Polymer Blend Dielectrics in Top-Gate Organic Field-Effect Transistors for Low-Voltage-Operating Complementary Circuits. *ACS Appl. Mater. Interfaces* **2012**, *4*, 6176−6184.

(10) Park, K.-I.; Bae, S. B.; Yang, S. H.; Lee, H. I.; Lee, K.; Lee, S. J. Lead-Free $BaTiO_3$ Nanowires-Based Flexible Nanocomposite Generator. *Nanoscale* **2014**, *6*, 8962−8968.

(11) Zhang, M.; Gao, T.; Wang, J.; Liao, J.; Qiu, Y.; Yang, Q.; Xue, H.; Shi, Z.; Zhao, Y.; Xiong, Z.; Chen, L. A Hybrid Fibers Based Wearable Fabric Piezoelectric Nanogenerator for Energy Harvesting Application. *Nano Energy* **2015**, *13*, 298−305.

(12) Dang, Z.-M.; Yuan, J.-K.; Zha, J.-W.; Zhou, T.; Li, S.-T.; Hu, G.-H. Fundamentals, Processes and Applications of High-Permittivity Polymer-Matrix Composites. *Prog. Mater. Sci.* **2012**, *57*, 660−723.

(13) Li, J. Y.; Zhang, L.; Ducharme, S. Electric Energy Density of Dielectric Nanocomposites. *Appl. Phys. Lett.* **2007**, *90*, 132901/1−132901/3.

(14) Claude, J.; Lu, Y.; Li, K.; Wang, Q. Electrical Storage in Poly(vinylidene fluoride) Based Ferroelectric Polymers: Correlating Polymer Structure to Electrical Breakdown Strength. *Chem. Mater.* **2008**, *20*, 2078−2080.

(15) Zhu, L.; Wang, Q. Novel Ferroelectric Polymers for High Energy Density and Low Loss Dielectrics. *Macromolecules* **2012**, *45*, 2937−2954.

(16) Huang, X.; Jiang, P. Core-Shell Structured High-*k* Polymer Nanocomposites for Energy Storage and Dielectric Applications. *Adv. Mater.* **2015**, *27*, 546−554.

(17) Li, J.; Claude, J.; Norena-Franco, L. E.; Seok, S. I.; Wang, Q. Electrical Energy Storage in Ferroelectric Polymer Nanocomposites Containing Surface-Functionalized $BaTiO_3$ Nanoparticles. *Chem. Mater.* **2008**, *20*, 6304−6306.

(18) Li, Q.; Zhang, G.; Liu, F.; Han, K.; Gadinski, M. R.; Xiong, C.; Wang, Q. Solution-Processed Ferroelectric Terpolymer Nanocomposites with High Breakdown Strength and Energy Density Utilizing Boron Nitride Nanosheets. *Energy Environ. Sci.* **2015**, *8*, 922−931.

(19) Yang, K.; Huang, X.; Fang, L.; He, J.; Jiang, P. Fluoro-Polymer Functionalized Graphene for Flexible Ferroelectric Polymer-Based High-*k* Nanocomposites with Suppressed Dielectric Loss and Low Percolation Threshold. *Nanoscale* **2014**, *6*, 14740−14753.

(20) Yang, K.; Huang, X.; Huang, Y.; Xie, L.; Jiang, P. Fluoro-Polymer@$BaTiO_3$ Hybrid Nanoparticles Prepared *via* RAFT Polymerization: Toward Ferroelectric Polymer Nanocomposites with High Dielectric Constant and Low Dielectric Loss for Energy Storage Application. *Chem. Mater.* **2013**, *25*, 2327−2338.

(21) Yang, K.; Huang, X.; Zhu, M.; Xie, L.; Tanaka, T.; Jiang, P. Combining RAFT Polymerization and Thiol-Ene Click Reaction for Core-Shell Structured Polymer@$BaTiO_3$ Nanodielectrics with High

DOI: 10.1021/acsami.5b06480
ACS Appl. Mater. Interfaces 2015, 7, 18017−18027

Dielectric Constant, Low Dielectric Loss and High Energy Storage Capability. *ACS Appl. Mater. Interfaces* **2014**, *6*, 1812−1822.
(22) Yang, K.; Huang, X.; Xie, L.; Wu, C.; Jiang, P.; Tanaka, T. Core-Shell Structured Polystyrene/$BaTiO_3$ Hybrid Nanodielectrics Prepared by in situ RAFT Polymerization: A Route to High Dielectric Constant and Low Loss Materials with Weak Frequency Dependence. *Macromol. Rapid Commun.* **2012**, *33*, 1921−1926.
(23) Zhu, M.; Huang, X.; Yang, K.; Zhai, X.; Zhang, J.; He, J.; Jiang, P. Energy Storage in Ferroelectric Polymer Nanocomposites Filled with Core-Shell Structured Polymer@$BaTiO_3$ Nanoparticles: Understanding the Role of Polymer Shells in the Interfacial Regions. *ACS Appl. Mater. Interfaces* **2014**, *6*, 19644−19654.
(24) Xie, L.; Huang, X.; Huang, Y.; Yang, K.; Jiang, P. Core-Shell Structured Hyperbranched Aromatic Polyamide/$BaTiO_3$ Hybrid Filler for Poly(vinylidene fluoride-trifluoroethylene-chlorofluoroethylene) Nanocomposites with the Dielectric Constant Comparable to That of Percolative Composites. *ACS Appl. Mater. Interfaces* **2013**, *5*, 1747−1756.
(25) Xie, L.; Huang, X.; Huang, Y.; Yang, K.; Jiang, P. Core@Double-Shell Structured $BaTiO_3$-Polymer Nanocomposites with High Dielectric Constant and Low Dielectric Loss for Energy Storage Application. *J. Phys. Chem. C* **2013**, *117*, 22525−22537.
(26) Xie, L.; Huang, X.; Wu, C.; Jiang, P. Core-Shell Structured Poly(methyl methacrylate)/$BaTiO_3$ Nanocomposites Prepared by in situ Atom Transfer Radical Polymerization: A Route to High Dielectric Constant Materials with the Inherent Low Loss of the Base Polymer. *J. Mater. Chem.* **2011**, *21*, 5897−5906.
(27) Xie, L.; Huang, X.; Yang, K.; Li, S.; Jiang, P. "Grafting to" Route to PVDF-HFP-GMA/$BaTiO_3$ Nanocomposites with High Dielectric Constant and High Thermal Conductivity for Energy Storage and Thermal Management Applications. *J. Mater. Chem. A* **2014**, *2*, 5244−5251.
(28) Xie, L.; Huang, X.; Li, B.-W.; Zhi, C.; Tanaka, T.; Jiang, P. Core-Satellite Ag@$BaTiO_3$ Nanoassemblies for Fabrication of Polymer Nanocomposites with High Discharged Energy Density, High Breakdown Strength and Low Dielectric Loss. *Phys. Chem. Chem. Phys.* **2013**, *15*, 17560−17569.
(29) Kim, P.; Jones, S. C.; Hotchkiss, P. J.; Haddock, J. N.; Kippelen, B.; Marder, S. R.; Perry, J. W. Phosphonic Acid-Modified Barium Titanate Polymer Nanocomposites with High Permittivity and Dielectric Strength. *Adv. Mater.* **2007**, *19*, 1001−1005.
(30) Kim, P.; Zhang, X. H.; Domercq, B.; Jones, S. C.; Hotchkiss, P. J.; Marder, S. R.; Kippelen, B.; Perry, J. W. Solution-Processible High-Permittivity Nanocomposite Gate Insulators for Organic Field-Effect Transistors. *Appl. Phys. Lett.* **2008**, *93*, 013302/1−013302/3.
(31) Kim, P.; Doss, N. M.; Tillotson, J. P.; Hotchkiss, P. J.; Pan, M.-J.; Marder, S. R.; Li, J.; Calame, J. P.; Perry, J. W. High Energy Density Nanocomposites Based on Surface-Modified $BaTiO_3$ and a Ferroelectric Polymer. *ACS Nano* **2009**, *3*, 2581−2592.
(32) Tang, H.; Lin, Y.; Sodano, H. A. Enhanced Energy Storage in Nanocomposite Capacitors through Aligned PZT Nanowires by Uniaxial Strain Assembly. *Adv. Energy Mater.* **2012**, *2*, 469−476.
(33) Tang, H.; Sodano, H. A. High Energy Density Nanocomposite Capacitors Using Non-Ferroelectric Nanowires. *Appl. Phys. Lett.* **2013**, *102*, 063901/1−063901/4.
(34) Tang, H.; Sodano, H. A. Ultra High Energy Density Nanocomposite Capacitors with Fast Discharge Using $Ba_{0.2}Sr_{0.8}TiO_3$ Nanowires. *Nano Lett.* **2013**, *13*, 1373−1379.
(35) Tang, H.; Lin, Y.; Sodano, H. A. Synthesis of High Aspect Ratio $BaTiO_3$ Nanowires for High Energy Density Nanocomposite Capacitors. *Adv. Energy Mater.* **2013**, *3*, 451−456.
(36) Tang, H.; Zhou, Z.; Sodano, H. A. Relationship between $BaTiO_3$ Nanowire Aspect Ratio and the Dielectric Permittivity of Nanocomposites. *ACS Appl. Mater. Interfaces* **2014**, *6*, 5450−5455.
(37) Liu, S.; Zhai, J.; Wang, J.; Xue, S.; Zhang, W. Enhanced Energy Storage Density in Poly(vinylidene fluoride) Nanocomposites by a Small Loading of Surface-Hydroxylated $Ba_{0.6}Sr_{0.4}TiO_3$ Nanofibers. *ACS Appl. Mater. Interfaces* **2014**, *6*, 1533−1540.
(38) Liu, S.; Zhai, J. Improving the Dielectric Constant and Energy Density of Poly(vinylidene fluoride) Composites Induced by Surface-Modified $SrTiO_3$ Nanofibers by Polyvinylpyrrolidone. *J. Mater. Chem. A* **2015**, *3*, 1511−1517.
(39) Wang, Z.; Nelson, J. K.; Hillborg, H.; Zhao, S.; Schadler, L. S. Dielectric Constant and Breakdown Strength of Polymer Composites with High Aspect Ratio Fillers Studied by Finite Element Models. *Compos. Sci. Technol.* **2013**, *76*, 29−36.
(40) Wang, Z.; Nelson, J. K.; Miao, J.; Linhardt, R. J.; Schadler, L. S.; Hillborg, H.; Zhao, S. Effect of High Aspect Ratio Filler on Dielectric Properties of Polymer Composites: A Study on Barium Titanate Fibers and Graphene Platelets. *IEEE Trans. Dielectr. Electr. Insul.* **2012**, *19*, 960−967.
(41) Song, Y.; Shen, Y.; Liu, H.; Lin, Y.; Li, M.; Nan, C.-W. Enhanced Dielectric and Ferroelectric Properties Induced by Dopamine-Modified $BaTiO_3$ Nanofibers in Flexible Poly(vinylidene fluoride-trifluoroethylene) Nanocomposites. *J. Mater. Chem.* **2012**, *22*, 8063−8068.
(42) Song, Y.; Shen, Y.; Liu, H.; Lin, Y.; Li, M.; Nan, C.-W. Improving the Dielectric Constants and Breakdown Strength of Polymer Composites: Effects of the Shape of the $BaTiO_3$ Nanoinclusions, Surface Modification and Polymer Matrix. *J. Mater. Chem.* **2012**, *22*, 16491−16498.
(43) Hu, P.; Song, Y.; Liu, H.; Shen, Y.; Lin, Y.; Nan, C.-W. Largely Enhanced Energy Density in Flexible P(VDF-TrFE) Nanocomposites by Surface-Modified Electrospun $BaSrTiO_3$ Fibers. *J. Mater. Chem. A* **2013**, *1*, 1688−1693.
(44) Zhao, B.; Lin, L.; He, D. Phase and Morphological Transitions of Titania/Titanate Nanostructures from an Acid to an Alkali Hydrothermal Environment. *J. Mater. Chem. A* **2013**, *1*, 1659−1668.
(45) Yin, J.; Qi, L.; Wang, H. Sodium Titanate Nanotubes as Negative Electrode Materials for Sodium-Ion Capacitors. *ACS Appl. Mater. Interfaces* **2012**, *4*, 2762−2768.
(46) Bao, N.; Shen, L.; Srinivasan, G.; Yanagisawa, K.; Gupta, A. Shape-Controlled Monocrystalline Ferroelectric Barium Titanate Nanostructures: From Nanotubes and Nanowires to Ordered Nanostructures. *J. Phys. Chem. C* **2008**, *112*, 8634−8642.
(47) Yang, D.; Tian, M.; Li, D.; Wang, W.; Ge, F.; Zhang, L. Enhanced Dielectric Properties and Actuated Strain of Elastomer Composites with Dopamine-Induced Surface Functionalization. *J. Mater. Chem. A* **2013**, *1*, 12276−12284.
(48) Arbatti, M.; Shan, X.; Cheng, Z. Y. Ceramic−Polymer Composites with High Dielectric Constant. *Adv. Mater.* **2007**, *19*, 1369−1372.
(49) Dang, Z.-M.; Lin, Y.-Q.; Xu, H.-P.; Shi, C.-Y.; Li, S.-T.; Bai, J. Fabrication and Dielectric Characterization of Advanced $BaTiO_3$/Polyimide Nanocomposite Films with High Thermal Stability. *Adv. Funct. Mater.* **2008**, *18*, 1509−1517.
(50) Dang, Z.-M.; Xu, H.-P.; Wang, H.-Y. Significantly Enhanced Low-Frequency Dielectric Permittivity in the $BaTiO_3$/Poly(vinylidene fluoride) Nanocomposite. *Appl. Phys. Lett.* **2007**, *90*, 012901.
(51) Huang, X.; Xie, L.; Jiang, P.; Wang, G.; Liu, F. Electrical, Thermophysical and Micromechanical Properties of Ethylene-Vinyl Acetate Elastomer Composites with Surface Modified $BaTiO_3$ nanoparticles. *J. Phys. D: Appl. Phys.* **2009**, *42*, 245407/1−245407/3.
(52) Huang, X.; Li, Y.; Liu, F.; Jiang, P.; Iizuka, T.; Tatsumi, K.; Tanaka, T. Electrical Properties of Epoxy/POSS Composites with Homogeneous Nanostructure. *IEEE Trans. Dielectr. Electr. Insul.* **2014**, *21*, 1516−1528.
(53) Zhang, X.; Shen, Y.; Zhang, Q.; Gu, L.; Hu, Y.; Du, J.; Lin, Y.; Nan, C.-W. Ultrahigh Energy Density of Polymer Nanocomposites Containing $BaTiO_3$@TiO_2 Nanofibers by Atomic-Scale Interface Engineering. *Adv. Mater.* **2015**, *27*, 819−824.
(54) Hu, P.; Shen, Y.; Guan, Y.; Zhang, X.; Lin, Y.; Zhang, Q.; Nan, C. W. Topological-Structure Modulated Polymer Nanocomposites Exhibiting Highly Enhanced Dielectric Strength and Energy Density. *Adv. Funct. Mater.* **2014**, *24*, 3172−3178.
(55) Song, Y.; Shen, Y.; Hu, P.; Lin, Y.; Li, M.; Nan, C. W. Significant Enhancement in Energy Density of Polymer Composites Induced by

DOI: 10.1021/acsami.5b06480
ACS Appl. Mater. Interfaces 2015, 7, 18017−18027

Dopamine-Modified $Ba_{0.6}Sr_{0.4}TiO_3$ Nanofibers. *Appl. Phys. Lett.* **2012**, *101*, 152904/1−152904/3.
(56) Tomer, V.; Randall, C. A.; Polizos, G.; Kostelnick, J.; Manias, E. High- and Low-Field Dielectric Characteristics of Dielectrophoretically Aligned Ceramic/Polymer Nanocomposites. *J. Appl. Phys.* **2008**, *103*, 034115.
(57) Li, J.; Seok, S. I.; Chu, B.; Dogan, F.; Zhang, Q.; Wang, Q. Nanocomposites of Ferroelectric Polymers with TiO_2 Nanoparticles Exhibiting Significantly Enhanced Electrical Energy Density. *Adv. Mater.* **2009**, *21*, 217−221.
(58) Ma, D.; Hugener, T. A.; Siegel, R. W.; Christerson, A.; Martensson, E.; Oenneby, C.; Schadler, L. S. Influence of Nanoparticle Surface Modification on the Electrical Behaviour of Polyethylene Nanocomposites. *Nanotechnology* **2005**, *16*, 724−731.
(59) Adikary, S. U.; Chan, H. L. W. Ferroelectric and Dielectric Properties of Sol−Gel Derived $Ba_xSr_{1-x}TiO_3$ Thin Films. *Thin Solid Films* **2003**, *424*, 70−74.

DOI: 10.1021/acsami.5b06480
ACS Appl. Mater. Interfaces 2015, 7, 18017−18027